

# Photoinduced interfacial chiral modes in threefold topological semimetal

SK Firoz Islam<sup>1</sup> and A. A. Zyuzin<sup>1,2</sup>

<sup>1</sup>*Department of Applied Physics, Aalto University, P.O. Box 15100, FI-00076 AALTO, Finland*

<sup>2</sup>*Ioffe Physical-Technical Institute, 194021 Saint Petersburg, Russia*



(Received 25 July 2019; published 7 October 2019)

We investigate the chiral electronic modes at the interface between two regions of a threefold topological semimetal, which is illuminated by left and right handed elliptically polarized waves. The radiation effects on the band structure of semimetal are analyzed by using Floquet theory. Two distinct solutions of the interface modes are found with the chirality depending on the phase of the irradiation. We also consider the anomalous Hall response, which is attributed to the interband contribution between the dispersionless flat band and conic bands.

DOI: [10.1103/PhysRevB.100.165302](https://doi.org/10.1103/PhysRevB.100.165302)

## I. INTRODUCTION

Recently, the possibility of manipulating the electronic band structure by applying a time-dependent periodic perturbation in the form of irradiation/light has received much attention, especially after the proposals of light induced topological phase transition [1–10] (the Floquet topological insulator), which has also been confirmed by experiments [11–13]. There is also a series of works [14–18] predicting phototunable Weyl nodes. Apart from these, optical pumping can also be used to control the spin and the valley degree of freedom in Dirac materials [19–22], which is the key requirement for the spin and valleytronics. Moreover, electromagnetic field can play the key role in  $0 - \pi$  phase transition in Josephson current in a normal-superconductor-normal (NSN) hybrid junction made of silicene [23] and Weyl semimetal [24].

Topological semimetals with multiple bands have recently been predicted [25,26]. These materials are also known as multifold semimetals and can be described by the higher number (more than two) of band crossing degeneracy, which differs itself from the linear dispersion at the nodal band-touching points in Weyl semimetal. Several experiments [27–30] have also confirmed the existence of such multifold semimetals. It has recently been found that multifold fermions are very promising in exhibiting the quantized photogalvanic effect [31,32]. The signature of multifold bands in such materials has also been explored in optical conductivity [33].

We particularly focus on threefold semimetal, which can be considered as the three-dimensional (3D) analog of the two-dimensional (2D) dice lattice [34,35]. One of the distinct features of threefold semimetal is the existence of the dispersionless flat band, which has some unusual consequences in transport signature [36–38]. The effects of light/irradiation in the 2D dice lattice [21,39,40] have been investigated very recently. On the other hand, much less attention has been paid for 3D threefold semimetal in the context of its interaction with irradiation. It can be easily anticipated that shedding light can induce a mass term and subsequently opens a gap in the band dispersion, irrespective of the dimensionality. However, apart from the gap opening, irradiation can also induce a mo-

mentum shift along the extra dimension and that shifting can be manipulated in opposite directions in two different regions of the materials by controlling the phase of the irradiation. In this paper, we follow this route to induce opposite momentum shifting in two different regions by shedding irradiation with opposite phase. The effect of irradiation is included by means of Floquet theory [41] under the limit of high-frequency expansion (Floquet-Magnus expansion). We find that there exist two chiral interfacial surface modes and calculate the anomalous Hall conductivity induced due to irradiation.

The occurrence of analogous optical interfacial surface modes is a well-studied topic [42]. In optics, the interface of two optically active isotropic media with opposite sign of the gyrotropic coefficient supports unidirectional surface electromagnetic waves [43–45].

The remainder of the paper is presented as follows. Section II discusses the linearized Hamiltonian of the three-band model and its band dispersion with the effect of irradiation. The dispersion relations of chiral modes localized at the interface where the irradiation changes phase are obtained in Sec. III. Section IV is devoted to calculation of the anomalous Hall conductivity and the transparency region for irradiation. Finally, we summarize and conclude in Sec. V.

## II. THE MODEL AND FLOQUET THEORY

We start with the Hamiltonian, that describes the groups of space groups 199 and 214 materials as [25,33]

$$H_{3f} = v \begin{bmatrix} 0 & e^{i\phi} k_z & e^{-i\phi} k_y \\ e^{-i\phi} k_z & 0 & e^{i\phi} k_x \\ e^{i\phi} k_y & e^{-i\phi} k_x & 0 \end{bmatrix}, \quad (1)$$

where  $\phi$  is a real parameter,  $v$  is the Fermi velocity, and we use  $c = k_B = \hbar = 1$  throughout the calculations. We consider only a single nodal point in the first Brillouin zone. The band is nondegenerate except at  $k = 0$ , unless  $\phi = n\pi/3$  with  $n$  being an integer. Another noticeable point is that for  $\pi/3 < \phi < 2\pi/3$  the Hamiltonian is adiabatically connected to the one with  $\phi = \pi/2$ . The Hamiltonian at this point can be written as  $H_{3f} = v\mathbf{k} \cdot \mathbf{S}$  with  $S_{x,y,z}$  being the generators of

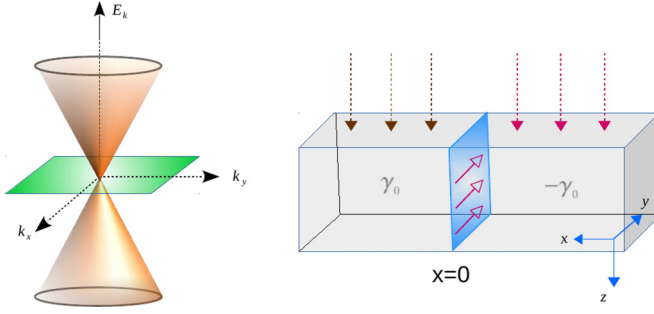


FIG. 1. Left: A sketch of the energy dispersion for threefold semimetals for  $k_z = 0$ . Right: A schematic sketch of the setup. Two regions are illuminated by the elliptically polarized irradiation of opposite handedness. Irradiation results in the domain wall at which parameter  $\gamma = \gamma_0[2\Theta(x) - 1]$  changes sign. The interface where  $\gamma = 0$  is shown by the blue plane at  $x = 0$ . The domain wall hosts unidirectional electronic modes, with the chirality indicated by arrows in this plane.

the rotation group  $SO(2)$  in the pseudospin-1 representation defined as

$$\mathbf{S} = i \begin{bmatrix} 0 & \hat{e}_z & -\hat{e}_y \\ -\hat{e}_z & 0 & \hat{e}_x \\ \hat{e}_y & -\hat{e}_x & 0 \end{bmatrix}. \quad (2)$$

We shall keep  $\phi = \pi/2$  throughout the whole paper. The energy spectrum is given by dispersive bands  $E_{\pm} = \pm vk$  and a dispersionless flat band  $E_0 = 0$ , which is shown in the left panel of Fig. 1. This is a 3D analog of a 2D dice lattice.

Let us now consider that the system is subjected to an external time-dependent periodic perturbation, moving along the  $z$  direction as shown by the arrow sign in the right panel of Fig. 1, which is described by a vector potential  $\mathbf{A}(t) = [A_x \sin(\Omega t), A_y \sin(\Omega t - \delta), 0]$ . Here  $\Omega$  is the frequency of the irradiation and  $\delta$  is the phase. The Hamiltonian describing threefold semimetal in the presence of radiation can be written by utilizing the Peierls substitution  $\mathbf{k} \rightarrow \mathbf{k} - e\mathbf{A}(t)$ , where  $e < 0$  is the electron charge, as

$$H_{3f}(t) = H_{3f} + V(t), \quad (3)$$

with

$$V(t) = -ev[S_x A_x \sin(\Omega t) + S_y A_y \sin(\Omega t - \delta)]. \quad (4)$$

The above Hamiltonian can be solved by using Floquet theory which states that the system under the time-dependent periodic perturbation exhibits a complete set of solutions of the form  $\psi(r, t) = \phi(r, t)e^{-iet}$  where  $\phi(r, t) = \phi(r, t + \mathcal{T})$  and  $\mathcal{T}$  is the periodicity of the field, the corresponding Floquet states [41]. It resembles the Bloch theorem in the momentum space. The Floquet eigenstates can be inserted into the time-dependent Schrödinger equation to obtain the Floquet eigenvalue equation as  $H_{3f}^F \phi(r, t) = \epsilon \phi(r, t)$  with  $H_{3f}^F = H_{3f}(t) - i\partial_t$ .

The Floquet eigenstates can be further expressed in Fourier form as  $\phi(r, t) = \sum_n \phi_n(r, t)e^{in\Omega t}$ , where  $n$  denotes the Fourier components or Floquet side bands. To obtain the Floquet energy spectrum, the Floquet Hamiltonian has to be diagonalized in the basis of the Floquet side band  $n$ . However,

in such case one must restrict the side band index by setting a cutoff. On the other hand, for the high-frequency regime of the field, an effective Hamiltonian can be obtained by following Floquet-Magnus expansion up to the second order in field amplitude as [41]

$$\tilde{H}_{3f} \simeq H_{3f} + \frac{[V_+, V_-]}{\Omega}, \quad (5)$$

where the second term describes the irradiation induced correction with

$$V_m = \frac{1}{\mathcal{T}} \int_0^{\mathcal{T}} V(t) e^{-im\Omega t} dt. \quad (6)$$

The effective Hamiltonian can be further simplified to

$$\tilde{H}_{3f} \simeq H_{3f} + S_z v \gamma, \quad (7)$$

where  $\gamma = ve^2(2\Omega)^{-1}A_x A_y \sin \delta$ . For linear polarizations,  $\gamma = 0$ . Note that the extra term in Eq. (7),  $S_z v \gamma$ , causes a momentum shift along the  $k_z$  direction that can be further seen in the energy spectrum of the irradiated system as  $E_{\pm} = \pm v \sqrt{(k_z + \gamma)^2 + k_x^2 + k_y^2}$ .

### III. INTERFACIAL MODES

In this section, we obtain the chiral modes propagating along the interface between two regions with different  $\gamma$ , following the analogy with optical evanescent modes [44]. The two regions of the material exposed to the external irradiation are schematically shown in Fig. 1. The phase factor of the wave is adjusted in such way that  $\gamma$  changes sign in two regions as

$$\gamma = \gamma_0[2\Theta(x) - 1], \quad (8)$$

where  $\gamma_0 = ve^2 A_x A_y / 2\Omega$ ,  $\Theta(x)$  is the step function, and  $\partial\gamma/\partial x = 2\gamma_0\delta(x)$ . We seek a solution of equation  $\tilde{H}_{3f}\Psi = E\Psi$  in the form  $\Psi = [\psi_1, \psi_2, \psi_3]^T e^{i(k_y y + k_z z)}$ , which explicitly gives

$$iv \begin{bmatrix} 0 & k_z + \gamma & -k_y \\ -k_z - \gamma & 0 & -i\partial_x \\ k_y & i\partial_x & 0 \end{bmatrix} \Psi = E\Psi. \quad (9)$$

It is instructive to rewrite the above equation as

$$\frac{\partial^2 \psi_2}{\partial x^2} + U(x)\psi_2 = \left\{ k_y^2 + [k_z + \gamma(x)]^2 - \frac{E^2}{v^2} \right\} \psi_2, \quad (10)$$

where  $U(x) = 2\gamma_0 v k_y \delta(x)/E$ . The above equation resembles the one-dimensional (1D) Schrödinger equation in a delta potential, which supports a bound state provided  $\gamma_0 v k_y / E > 0$ . By utilizing the continuity conditions for the wave function at the interface  $x = 0$ , one obtains an equation to determine the dispersion relation

$$\sum_{s=\pm} \left[ k_y^2 + (k_z + s\gamma_0)^2 - \frac{E^2}{v^2} \right]^{1/2} = 2\gamma_0 \frac{v k_y}{E}. \quad (11)$$

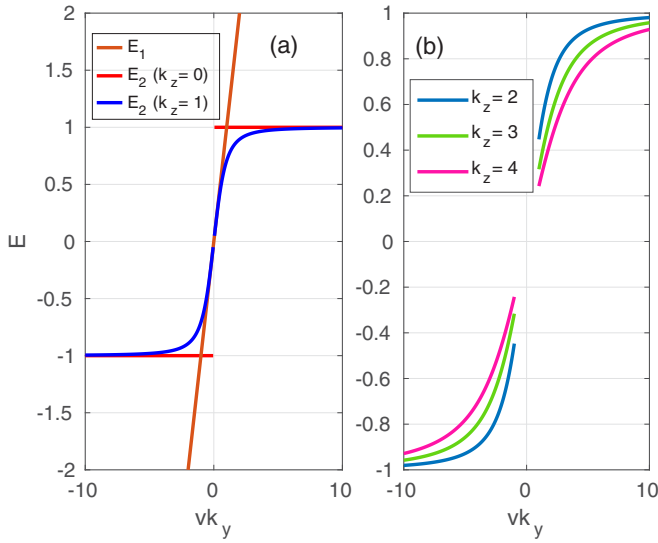


FIG. 2. At fixed  $\gamma_0 > 0$  (the energies are measured in the units of  $v\gamma_0$  and lengths in  $\gamma_0^{-1}$ ) in the model of abrupt interface, the chiral interface modes given by the solution of Eq. (10) for two different momenta (a)  $k_z \leq 1$ , where the dispersion of the chiral mode Eq. (12a) stays intact,  $E_1 = vk_y$ , while the flat band Eq. (12b) given by  $E_2(k_z = 0)$  acquires the curvature at  $k_z \neq 0$ , and (b)  $k_z > 1$ , where the mode Eq. (12a) disappears.

Two solutions of this equation exist provided inequality  $vk_y\gamma_0/E > 0$  holds:

$$E_1 = vk_y \text{sgn} \gamma_0, \quad (12a)$$

$$E_2 = \frac{vk_y\gamma_0}{\sqrt{k_y^2 + k_z^2}}. \quad (12b)$$

The first solution exists provided  $|\gamma_0| \geq |k_z|$ , while the second is determined in the region  $k_y^2 + k_z^2 > |\gamma_0 k_z|$ . Note that the chirality of the modes is defined by the sign of parameter  $\gamma_0$ . The first dispersion is chiral and independent of  $k_z$  explicitly but bounded in the region  $k_z \in [-|\gamma_0|, |\gamma_0|]$ , while the second one becomes flat at  $k_z = 0$ , as shown in Fig. 2(a). At finite values of momenta  $k_z$  the second mode acquires a curvature with  $k_y$  and this curvature increases further with  $k_z$  as shown in Fig. 2(b). For completeness we present the solution of Eq. (11) for finite  $k_z$  in Fig. 2. This figure contains two subplots in which Fig. 2(b) is for  $k_z > 1$  and Fig. 2(a) is for  $k_z \leq 1$ .

The wave function, which corresponds to the eigenvalue  $E_{1,2}$ , is proportional to  $\Psi_{1,2} \propto e^{-x/\ell_{1,2,+}}$  at  $x > 0$  and  $\Psi_{1,2} \propto e^{x/\ell_{1,2,-}}$  at  $x < 0$ . The localization lengths are given by  $\ell_{1,\pm} = |k_z \pm \gamma_0|^{-1}$  and  $\ell_{2,\pm} = |k_y^2 + k_z^2 \pm \gamma_0 k_z|^{-1} \sqrt{k_y^2 + k_z^2}$ . Knowing the expression for  $\Psi(x)$ , one can show that, for the most interesting low-energy mode Eq. (12a), the pseudospin  $\langle S_x \rangle \propto \Psi^\dagger S_x \Psi = 0$  and  $\langle S_y \rangle \propto \text{sgn}(\gamma_0)$  on both sides of the interface, while the  $z$  component changes sign as  $\langle S_z \rangle \propto \text{sgn}(k_y \gamma_0 x)$ .

So far we have addressed the scenario for an abrupt interface between two regions. However, in the realistic case, the interface may not be always abrupt but rather smooth, which may be modeled as

$$\gamma(x) = \gamma_0 \tanh(x/L), \quad (13)$$

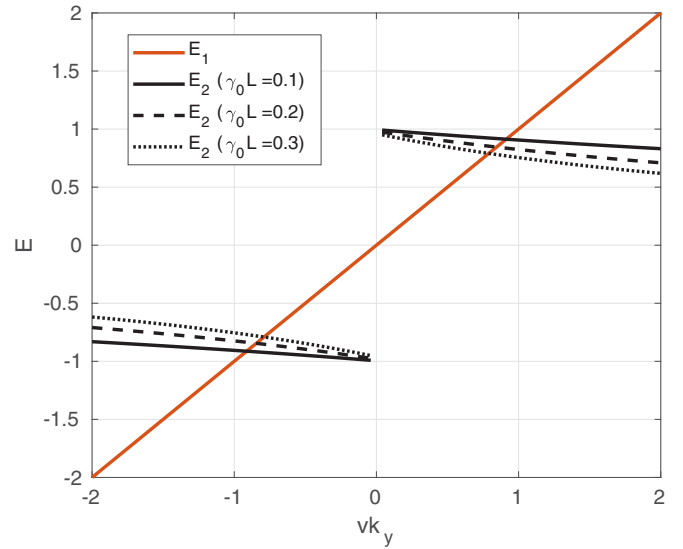


FIG. 3. At fixed  $\gamma_0$  and  $n = 0$ , the effect of smooth boundary on the dispersionless flat band and dispersive chiral modes are shown for different widths of the boundary.

where  $L$  is the typical barrier width. This yields the Schrödinger equation  $\partial_x^2 \psi_2 + [U_0 \text{sech}^2(x/L) - 2k_z \gamma_0 \tanh(x/L)] \psi_2 = (k_y^2 + k_z^2 + \gamma_0^2 - E^2/v^2) \psi_2$ , with  $U_0 = \frac{vk_y \gamma_0}{E} + \gamma_0^2$ . For simplicity at  $k_z = 0$ , by following the standard solution [46] one obtains the equation

$$\frac{E^2}{v^2} - k_y^2 - \gamma_0^2 = -\frac{1}{4L^2} [\sqrt{1 + 4L^2 U_0} - (2n + 1)]^2, \quad (14)$$

where  $n \in \mathbb{W}$  is bounded from above by the condition  $n < (-1 + \sqrt{1 + 4L^2 U_0})/2$ . Additionally, the smooth boundary also restricts the localized states through  $U_0 > 0$ . The number of allowed levels increases with the increase of  $L|\gamma_0|$ . The effect of the smooth boundary is plotted in Fig. 3 which shows that the band Eq. (12b) is affected by  $L$ . However, the spectrum of the chiral mode Eq. (12a) exists at  $n = 0$  and remains insensitive to the nature of the interface and is hence topological in nature. The modes which reside in  $n > 0$  are sensitive to the boundary details and nontopological in nature. For  $n^2 + n > \gamma_0^2 L^2$  one obtains low-energy chiral mode  $E \simeq \frac{\gamma_0 L v k_y}{n(n+1)}$ , while when  $n^2 + n < \gamma_0^2 L^2$  there is one more mode  $E \simeq v\gamma_0 - 2nvk_y(1 + \frac{1+n}{2\gamma_0 L})$ . We also note that the possible effects of finite thickness ( $L_z$ ) along the direction of propagation of light can be qualitatively captured by discretizing the momentum in this direction as  $k_z = n_z \pi / L_z$  with  $n_z \in \mathbb{Z}$ . We have also assumed that the thickness of the system along the  $z$  direction is much larger than  $1/|\gamma_0|$  and, hence, the amplitude and phase of the light are too weak to be considered. Finally we quickly comment here about the possible effects of  $k_z \neq 0$  on the smooth boundary solution. In such case, the effective confining potential around the interface is deformed and weakened, which can allow some of the modes (depending on  $E$  and  $k_z$ ) to penetrate inside the bulk.

The basic recipe of engineering such interfacial modes is the momentum shift along the  $k_z$  direction by applying irradiation. It is worthwhile to mention at this stage that the

topological electronic 1D chiral mode was predicted on the 2D surface of a 3D topological insulator (TI) [47] and optical modes bound at the domains in optical isomer systems [44]. The irradiation induced band-gap opening on the surface of the 3D TI plays the key role there. The present paper is based on 3D materials, where the external irradiation results in the momentum shift along the extra dimension.

#### IV. ANOMALOUS HALL RESPONSE

Let us now briefly discuss signatures of the irradiation in the response function. We particularly focus on anomalous Hall conductivity, which is exclusively attributed to the irradiation unlike longitudinal conductivity.

We should mention here that the expression for the current-current operator in the presence of the intense ac background has been formulated with the Floquet method in [1,48]. It was shown that the time-averaged operator can be written in terms of the Green's function, where the energies are replaced with the Floquet quasi-energies

$$\Pi_{xy}(\omega_m) = \text{tr} \sum_n T \int \frac{d^3k}{(2\pi)^3} G(i\omega_n + i\omega_m, \mathbf{k}) j_x G(i\omega_n, \mathbf{k}) j_y, \quad (15)$$

where the Green's function is given by

$$\begin{aligned} G(i\omega_n, \mathbf{k}) &= [i\omega_n + \mu - v\mathbf{S} \cdot \mathbf{k}]^{-1} \\ &= \frac{M_0(\mathbf{k})}{i\omega_n + \mu} + \frac{1}{2} \sum_{s=\pm} \frac{1 - M_0(\mathbf{k}) - isM_1(\mathbf{k})}{i\omega_n + \mu - svk}, \end{aligned} \quad (16)$$

with  $\mu$  is the chemical potential. The fermionic and bosonic Matsubara frequencies are denoted by  $\omega_n$  and  $\omega_m$ , respectively with  $n, m \in \mathcal{Z}$ . The different components of the Green's function are given by

$$M_0(\mathbf{k}) = \frac{1}{k^2} \begin{bmatrix} k_x^2 & k_x k_y & k_x k_z \\ k_x k_y & k_y^2 & k_y k_z \\ k_x k_z & k_y k_z & k_z^2 \end{bmatrix} \quad (17)$$

and

$$M_1(\mathbf{k}) = \frac{1}{k} \begin{bmatrix} 0 & k_z & -k_y \\ -k_z & 0 & k_x \\ k_y & -k_x & 0 \end{bmatrix}. \quad (18)$$

The first term in Eq. (16) corresponds to the dispersionless flat band whereas the second term corresponds to the conic bands. The components of the current density operator are given by  $j_\alpha = e\partial\tilde{H}_{3f}/\partial k_\alpha$ . At zero temperature, using  $k = \sqrt{k_\perp^2 + k_z^2}$ ,  $\int \frac{d^3k}{(2\pi)^3} \dots = \int_{-\Lambda_{\text{reg}}}^{\Lambda_{\text{reg}} - \gamma_0} \frac{dk_z}{2\pi} \int \frac{d^2k_\perp}{4\pi^2} \dots$  with  $\Lambda_{\text{reg}}$  introduced for the correct definition of the  $k_z$  integral, and performing analytical continuation  $i\omega_m \rightarrow \omega + i\delta$ , it is straightforward to arrive at the anomalous Hall conductivity  $\sigma_{xy} = \lim_{\omega \rightarrow 0} \Pi_{xy}(\omega)/i\omega$  as

$$\sigma_{xy} = \frac{e^2 \gamma_0}{2\pi^2}, \quad (19)$$

which is two times larger than anomalous Hall conductivity in the Weyl semimetal due to the doubling of the topological charge. The sign of  $\sigma_{xy}$  depends on the phase of the incident radiation. The anomalous Hall response can be also

interpreted through the topological invariant (Chern number) which can be easily obtained by considering the Brillouin zone as a cube made of a number of 2D slabs in the  $x$ - $y$  plane in momentum space. The  $z$  component of the Berry curvature for the conical bands  $\pm v|\mathbf{k} + \gamma\hat{e}_z|$  is given by  $\pm(k_z + \gamma)/|\mathbf{k} + \gamma\hat{e}_z|^3$ , which can be integrated out in momentum space to get the Chern number  $C = \pm \text{sgn}(k_z + \gamma)$  (the flat band is trivial).

Note that it is the contribution between the dispersionless flat band and conic band which causes such result. The inter- or intra-conic-band transition does not contribute to the anomalous Hall conductivity, as the corresponding matrix element vanishes in the polarization operator in Eq. (15). We also mention here that the above formalism is well justified as long as we treat the irradiated Hamiltonian via Floquet-Magnus high-frequency approximation, where only the two nearest side bands are taken into account. It is instructive to adjust the chemical potential near to the band touching point in order to avoid any interference of higher Floquet side bands. To capture higher side bands, one must consider beyond high-frequency approximation and Floquet Green's-function approach for transport study [1].

For completeness, we also comment on the diagonal components of the polarization matrix at zero temperature and wave vector, which reduces to

$$\Pi_{xx} = \frac{\omega_m^2}{6\pi^2 v} \left[ \ln \frac{\Lambda^2}{\mu^2 + \omega_m^2} + \frac{\mu^2}{\omega_m^2} \right], \quad (20)$$

where  $\Lambda$  is the energy cutoff and the diamagnetic contribution has been subtracted. The effect of the flat band is to render the valence to conduction interband transitions, which leads to the imaginary component already at  $\omega = \mu$ . This is in contrast to the  $\omega = 2\mu$  condition in 3D Weyl semimetals. The transparency region to the external irradiation can be estimated by considering the conditions for the zero imaginary part and positive real components of the dielectric function. These require frequencies of the incident wave to be confined in the interval

$$\mu > \omega \geq \frac{\alpha\mu}{(1 + \alpha^2 \ln |\Lambda/\mu\sqrt{1 - \alpha^2}|)^{1/2}}, \quad (21)$$

with  $\alpha = N/(6\pi^2 v\epsilon_0)$  in which  $\epsilon_0$  is the permittivity of free space and  $N$  is the number of threefold band touching points.

#### V. DISCUSSION AND CONCLUSIONS

Let us estimate the parameters of the model. Typically, one can use the standard parameters of irradiation in the high-frequency limit as  $evA = 0.1$ – $1$  eV and  $0.1 < evA/\Omega < 1$ . Under this regime, we can estimate  $v\gamma_0 = v^2 e^2 A_x A_y / 2\Omega \approx 0.5(eAv/2) = 0.12$  eV. The frequency  $\Omega$  can be estimated to be  $\approx 200$  THz for  $eAv = 0.5$  eV, which gives the wavelength of the irradiation as  $1.2 \mu\text{m}$ .

To summarize, we present a theoretical proposal of engineering a unidirectional mode propagating along the interface between two regions of threefold semimetal. The band structure of such material in the presence of the irradiation is obtained within the Floquet theory in the high-frequency limit treating external field as a perturbation within the Floquet-Magnus expansion.

It is shown that time-dependent periodic perturbation, in the form of an elliptically polarized field in the  $x$ - $y$  plane, can cause a momentum shift along the  $k_z$  direction in the electronic band structure. By utilizing several sources of irradiation, domain walls might be realized in the material at which the phase factor of the field changes. It is found that the interface between two regions, exposed to the irradiation with opposite phase, can host a unidirectional Fermi-arc mode in addition to a dispersionless flat mode. The anomalous Hall conductivity and frequency interval at which the material

becomes transparent to irradiation by evaluating the dielectric tensor are discussed. Finally, it is also noted that spin orientation along the normal to the interface is zero while in the plane of the interface it flips across the interface.

### ACKNOWLEDGMENTS

This work is supported by the Academy of Finland. A.A.Z. is grateful to the hospitality of the Pirinem School of Theoretical Physics.

- 
- [1] T. Oka and H. Aoki, Photovoltaic Hall effect in graphene, *Phys. Rev. B* **79**, 081406(R) (2009).
- [2] N H Lindner, G. Refael, and V. Galitski, Floquet topological insulator in semiconductor quantum wells, *Nat. Phys.* **7**, 490 (2011).
- [3] J. I. Inoue and A. Tanaka, Photoinduced spin Chern number change in a two-dimensional quantum spin Hall insulator with broken spin rotational symmetry, *Phys. Rev. B* **85**, 125425 (2012).
- [4] T. Kitagawa, T. Oka, A. Brataas, L. Fu, and E. Demler, Transport properties of nonequilibrium systems under the application of light: Photoinduced quantum Hall insulators without Landau levels, *Phys. Rev. B* **84**, 235108 (2011).
- [5] A. López, Z. Z. Sun, and J. Schliemann, Floquet spin states in graphene under ac-driven spin-orbit interaction, *Phys. Rev. B* **85**, 205428 (2012).
- [6] X. Zhai and G. Jin, Photoinduced topological phase transition in epitaxial graphene, *Phys. Rev. B* **89**, 235416 (2014).
- [7] K. Saha, Photoinduced Chern insulating states in semi-Dirac materials, *Phys. Rev. B* **94**, 081103(R) (2016).
- [8] M. Ezawa, Photoinduced Topological Phase Transition and a Single Dirac-Cone State in Silicene, *Phys. Rev. Lett.* **110**, 026603 (2013).
- [9] P. M. Perez-Piskunow, G. Usaj, C. A. Balseiro, and L. E. F. Foa Torres, Floquet chiral edge states in graphene, *Phys. Rev. B* **89**, 121401(R) (2014).
- [10] J. Cayssol, B. Dóra, F. Simon, and R. Moessner, Floquet topological insulators, *Phys. Status Solidi* **7**, 101 (2013).
- [11] Y.-G. Peng, C.-Z. Qin, D.-G. Zhao, Y.-X. Shen, X.-Y. Xu, M. Bao, H. Jia, and X.-F. Zhu, Experimental demonstration of anomalous Floquet topological insulator for sound, *Nat. Commun.* **7**, 13368 (2016).
- [12] H. Zhang, J. Yao, J. Shao, H. Li, S. Li, D. Bao, C. Wang, and G. Yang, Anomalous photoelectric effect of a polycrystalline topological insulator film, *Sci. Rep.* **4**, 5876 (2014).
- [13] Y. Wang, H. Steinberg, P. Jarillo-Herrero, and N. Gedik, Observation of Floquet-Bloch states on the surface of a topological insulator, *Science* **342**, 453 (2013).
- [14] Z. Yan and Z. Wang, Tunable Weyl Points in Periodically Driven Nodal Line Semimetals, *Phys. Rev. Lett.* **117**, 087402 (2016).
- [15] X.-X. Zhang, T. T. Ong, and N. Nagaosa, Theory of photoinduced Floquet Weyl semimetal phases, *Phys. Rev. B* **94**, 235137 (2016).
- [16] B. Zhou, R. Chen, and D.-H. Xu, Floquet Weyl semimetals in light-irradiated type-II and hybrid line-node semimetals, *Phys. Rev. B* **97**, 155152 (2018).
- [17] A. Narayan, Tunable point nodes from line-node semimetals via application of light, *Phys. Rev. B* **94**, 041409(R) (2016).
- [18] M. Ezawa, Photoinduced topological phase transition from a crossing-line nodal semimetal to a multiple-Weyl semimetal, *Phys. Rev. B* **96**, 041205(R) (2017).
- [19] A. Kundu, H. A. Fertig, and B. Seradjeh, Floquet-Engineered Valleytronics in Dirac Systems, *Phys. Rev. Lett.* **116**, 016802 (2016).
- [20] L. E. Golub, S. A. Tarasenko, M. V. Entin, and L. I. Magarill, Valley separation in graphene by polarized light, *Phys. Rev. B* **84**, 195408 (2011).
- [21] B. Dey and T. K. Ghosh, Photoinduced valley and electron-hole symmetry breaking in  $\alpha - T_3$  lattice: The role of a variable Berry phase, *Phys. Rev. B* **98**, 075422 (2018).
- [22] M. Tahir, A. Manchon, and U. Schwingenschlögl, Photoinduced quantum spin and valley Hall effects, and orbital magnetization in monolayer MoS<sub>2</sub>, *Phys. Rev. B* **90**, 125438 (2014).
- [23] X. Zhou and G. Jin, Light-modulated  $0-\pi$  transition in a silicene-based Josephson junction, *Phys. Rev. B* **94**, 165436 (2016).
- [24] U. Khanna, S. Rao, and A. Kundu,  $0-\pi$  transitions in a Josephson junction of an irradiated Weyl semimetal, *Phys. Rev. B* **95**, 201115(R) (2017).
- [25] B. Bradlyn, J. Cano, Z. Wang, M. G. Vergniory, C. Felser, R. J. Cava, and B. A. Bernevig, Beyond Dirac and Weyl fermions: Unconventional quasiparticles in conventional crystals, *Science* **353**, aaf5037 (2016).
- [26] P. Tang, Q. Zhou, and S.-C. Zhang, Multiple Types of Topological Fermions in Transition Metal Silicides, *Phys. Rev. Lett.* **119**, 206402 (2017).
- [27] D. Takane, Z. Wang, S. Souma, K. Nakayama, T. Nakamura, H. Oinuma, Y. Nakata, H. Iwasawa, C. Cacho, T. Kim, K. Horiba, H. Kumigashira, T. Takahashi, Y. Ando, and T. Sato, Observation of Chiral Fermions with a Large Topological Charge and Associated Fermi-Arc Surface States in CoSi, *Phys. Rev. Lett.* **122**, 076402 (2019).
- [28] Z. Rao, H. Li, T. Zhang, S. Tian, C. Li, B. Fu, C. Tang, L. Wang, Z. Li, W. Fan, J. Li, Y. Huang, Z. Liu, Y. Long, C. Fang, H. Weng, Y. Shi, H. Lei, Y. Sun, T. Qian, and H. Ding, Observation of unconventional chiral fermions with long Fermi arcs in CoSi, *Nature (London)* **567**, 496 (2019).
- [29] D. S. Sanchez, I. Belopolski, T. A. Cochran, X. Xitong, J.-X. Yin, G. Chang, W. Xie, K. Manna, S. Vicky, C.-Y. Huang, N. Alidoust, D. Multer, S. S. Zhang, N. Shumiya, X. Wang, G.-Q. Wang, T.-R. Chang, C. Felser, S.-Y. Xu, S. Jia, H. Lin, and M. Z. Hassan, Topological chiral crystals with helicoid-arc quantum states, *Nature (London)* **567**, 500 (2019).

- [30] N. B. M. Schröter, D. Pei, M. G. Vergniory, Y. Sun, K. Manna, F. d. Juan, J. A. Krieger, V. Süss, M. Schmidt, P. Dudin, B. Bradlyn, T. K. Kim, T. Schmidt, C. Cacho, C. Felser, V. N. Stokov, and Y. Chen, Chiral topological semimetal with multifold band crossings and long Fermi arcs, *Nat. Phys.* **15**, 759 (2019).
- [31] G. Chang, S.-Y. Xu, B. J. Wieder, D. S. Sanchez, S.-M. Huang, I. Belopolski, T.-R. Chang, S. Zhang, A. Bansil, H. Lin, and M. Z. Hasan, Unconventional Chiral Fermions and Large Topological Fermi Arcs in RhSi, *Phys. Rev. Lett.* **119**, 206401 (2017).
- [32] F. Flicker, F. de Juan, B. Bradlyn, T. Morimoto, M.-G. Vergniory, and A.-G. Grushin, Chiral optical response of multifold fermions, *Phys. Rev. B* **98**, 155145 (2018).
- [33] M.-A. Sánchez-Martínez, F. de Juan, and A. G. Grushin, Linear optical conductivity of chiral multifold fermions, *Phys. Rev. B* **99**, 155145 (2019).
- [34] B. Dóra, J. Kailasvuori, and R. Moessner, Lattice generalization of the Dirac equation to general spin and the role of the flat band, *Phys. Rev. B* **84**, 195422 (2011).
- [35] A. Raoux, M. Morigi, J.-N. Fuchs, F. Piéchon, and G. Montambaux, From Dia- to Paramagnetic Orbital Susceptibility of Massless Fermions, *Phys. Rev. Lett.* **112**, 026402 (2014).
- [36] M. Vigh, L. Oroszlány, S. Vajna, P. San-Jose, G. Dávid, J. Cserti, and B. Dóra, Diverging DC conductivity due to a flat band in a disordered system of pseudospin-1 Dirac-Weyl fermions, *Phys. Rev. B* **88**, 161413(R) (2013).
- [37] J. D. Malcolm and E. J. Nicol, Magneto-optics of massless Kane fermions: Role of the flat band and unusual Berry phase, *Phys. Rev. B* **92**, 035118 (2015).
- [38] T. Biswas and T. K. Ghosh, Magnetotransport properties of the  $\alpha$ -T<sub>3</sub> model, *J. Phys.: Cond. Mat.* **28**, 495302 (2016).
- [39] B. Dey and T. K. Ghosh, Floquet topological phase transition in the  $\alpha - T_3$  lattice, *Phys. Rev. B* **99**, 205429 (2019).
- [40] A. Iurov, G. Gumbs, and D. Huang, Peculiar electronic states, symmetries, and berry phases in irradiated  $\alpha - T_3$  materials, *Phys. Rev. B* **99**, 205135 (2019).
- [41] A. Eckardt, Colloquium: Atomic quantum gases in periodically driven optical lattices, *Rev. Mod. Phys.* **89**, 011004 (2017).
- [42] A. Yariv and P. Yeh, *Optical Waves in Crystal* (Wiley, New York, 1984).
- [43] S. R. Seshadri, Excitation of surface waves on a perfectly conducting screen covered with anisotropic plasma, *IRE Trans. Microw. Theory Tech.* **10**, 573 (1962).
- [44] L. E. Zhukov and M. E. Raikh, Chiral electromagnetic waves at the boundary of optical isomers: Quantum Cotton-Mouton effect, *Phys. Rev. B* **61**, 12842 (2000).
- [45] A. A. Zyuzin and V. A. Zyuzin, Chiral electromagnetic waves in Weyl semimetals, *Phys. Rev. B* **92**, 115310 (2015).
- [46] L. D. Landau and E. M. Lifshitz, *Quantum Mechanics* (Pergamon, New York, 1977).
- [47] H. L. Calvo, L. E. F. Foa Torres, P. M. Perez-Piskunow, C. A. Balseiro, and G. Usaj, Floquet interface states in illuminated three-dimensional topological insulators, *Phys. Rev. B* **91**, 241404(R) (2015).
- [48] A. Menon, D. Chowdhury, and B. Basu, Photoinduced tunable anomalous Hall and Nernst effects in tilted Weyl semimetals using Floquet theory, *Phys. Rev. B* **98**, 205109 (2018).